JTTEE5 10:367-374

Peening Action and Residual Stresses in High-Velocity Oxygen Fuel Thermal Spraying of 316L Stainless Steel

Seiji Kuroda, Yasuhiko Tashiro, Hisami Yumoto, Susumu Taira, Hirotaka Fukanuma, and Shogo Tobe

(Submitted 7 March 2000; in revised form 7 July 2000)

316L stainless steel powder was sprayed by a high-pressure high-velocity oxygen fuel (HVOF) process. Effects of powder size and the pressure in the combustion chamber on the velocity and temperature of sprayed particles were studied by using an optical instrument, first, at the substrate position. A strong negative correlation between the particle temperature and the diameter was found, whereas the correlation between the velocity and the diameter was not significant. The pressure in the combustion chamber affected the velocity of sprayed particles significantly, whereas the particle temperature remained largely unchanged. *In-situ* curvature measurement was employed in order to study the process of stress generation during HVOF spraying. From the measured curvature changes, the intensity of peening action and the resultant compressive stress by HVOF sprayed particles were found to increase with the kinetic energy of the sprayed particles. The results were further used to estimate the stress distribution within the coatings. X-ray stress measurement revealed that the residual stress on the surface of the HVOF coatings is low and often in tension, but the stress inside the coatings is in a high level of compression.

Keywords 316L stainless steel, curvature measurement, HVOF, residual stress, sprayed coating, x-ray stress measurement

1. Introduction

Stress generation during high-velocity oxygen fuel (HVOF) thermal spray was studied in a previous report by using the *in-situ* curvature monitoring technique.[1] 316L stainless steel, Hastelloy C, and WC-12% Co were sprayed onto 316L stainless steel substrates by a high-pressure HVOF system under the conditions near those recommended by the manufacturer (TAFA, Concord, NH). It was found that the curvature changes through three stages: (1) abrupt change at the onset of spraying, (2) continuous change during spraying, and (3) change due to the mismatch in the thermal expansivity between the coating and the substrate during cooling after spraying. Compressive stress ranging from 70 to 420 MPa was found to be generated during spraying due to the "peening effect" of the HVOF sprayed particles at high velocity and in poorly molten state. Itoh *et al*. also reported generation of compressive stress in HVOF sprayed MCrAlY alloys by using a cantilever deflection method.[2]

These results have led us to a more generalized model of stress generation by thermally sprayed particles, as shown in Fig. 1. In conventional thermal spray processes, the majority of sprayed particles are molten before impact and the velocity of particles is below 300 m/s. As shown in Fig. 1(a), molten particles are flattened upon impact and quenched. After solidification, thermal contraction of each splat is constrained by the underlying solid, and tensile stress is generated within the splat as it cools to the substrate temperature. The nature of this "quenching stress" has been studied extensively including its dependence on the powder material and substrate temperature.[3,4] One important trait of the quenching stress is that it is independent of the substrate material, which significantly simplifies the modeling of the stress generation process and calculation of the stress distribution.[5,6]

In contrast, the temperature of sprayed particles in HVOF thermal spray is often somewhat below the melting point of the powder material, while the velocity of the particles exceeds 500 m/s. Therefore, the kinetic energy of sprayed particles plays a significant role upon impact by plastically deforming the surface layer of the target and inducing a significant level of compressive stress, as shown in Fig. 1(b). This process is analogous to shot peening, except that, in HVOF thermal spray, the particle is hot and sticks to the target. The stress state in the particle on top may be tensile due to the quenching stress. Hence, at least three parameters are necessary to characterize the stress distribution set by the impact of a HVOF particle, *i.e.*, the quenching stress σ_q in the particle itself, the peak magnitude of the peening stress σ_p, and the depth δ_p of penetration. Since σ_p and δ_p depend on the properties of both the impinging particles and the target material, more complicated stress behavior is expected as a coating builds up on the substrate.

In this study, *in-situ* curvature measurement of a substrate during spraying is employed in combination with a diagnostic instrument for sprayed particles in order to investigate the relationship between the conditions of sprayed particles in flight and the stress generation during deposition. In order to focus on the compressive peening stress, 316L stainless steel is employed for

Seiji Kuroda, National Institute for Materials Science, Tsukuba, Ibaraki, Japan; **Yasuhiko Tashiro** and **Hisami Yumoto,** Science University of Tokyo, Noda, Chiba, Japan; **Susumu Taira** and **Hirotaka Fukanuma,** Plasma Giken Co. Ltd., Toda, Saitama, Japan; and **Shogo Tobe,** Ashikaga Institute of Technology, Ashikaga, Tochigi, Japan. Contact e-mail: seiji.KURODA@nims.go.jp.

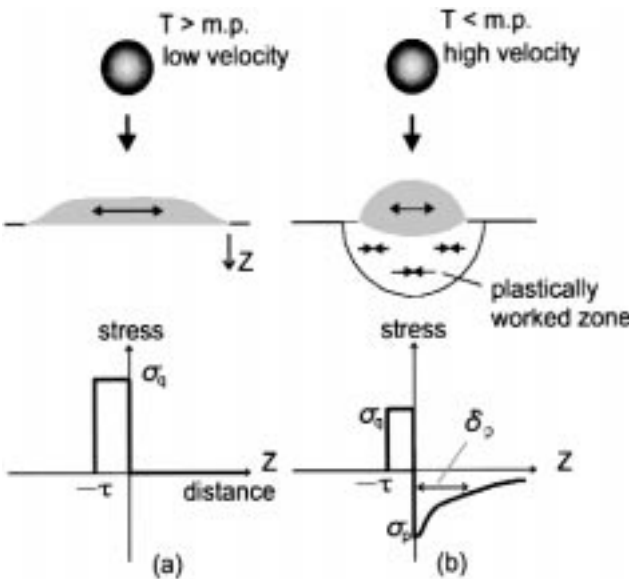

Fig. 1 Schematic of stress generation by a thermally sprayed particle: (**a**) molten particle and (**b**) not molten particle

both the spray powder and the substrates to eliminate the stress due to the difference in thermal expansivity between the coating and the substrate. Powder size and the velocity of sprayed particles are varied in order to control the kinetic energy of particles upon impact.

2. Experimental Procedures

2.1 Coating Deposition

A high-pressure HVOF spray system JP-5000 (TAFA, Concord, NH) was used to spray 316L stainless steel powders. The conditions are listed in Table 1, which shows the S and V series. For the S-series experiments, original powder (MA31, Showa Denko (Tokyo, Japan)) with 10 to 74 μm size distribution was sieved into three ranges, *i.e.*, 10 to 25 (S1), 25 to 53 (S2), and 53 to 74 μm (S3). In the V series, the combustion chamber pressure was varied by changing both the fuel (kerosene) and oxygen flow rates while maintaining the stoichiometry, which was intended to change the mean velocity of sprayed particles.[7] The equivalence fuel/oxygen ratio Φ is a normalized mass ratio of fuel flow with respect to oxygen and $\Phi = 1$ corresponds to the stoichiometry for complete combustion.[7]

2.2 In-Flight Particle Diagnostics

A diagnostic system DPV-2000 (TECNAR Quebec, Canada) was employed in order to measure the temperature, velocity, and size of HVOF sprayed particles at the center of the particle flux at the substrate position, *i.e.*, 380 mm downstream from the nozzle exit. The system collects the thermal radiation emitted by individual sprayed particles in flight through a pair of slits and analyzes its waveform at two wavelengths. The particle velocity is derived from the waveform analysis, the temperature is determined by two-color pyrometry, and the diameter is measured by the intensity of the signal.[8]

2.3 Curvature Measurement

The curvature of a substrate and its temperature were continuously measured by an instrument reported previously.[9] Substrates were 316L stainless steel plates $2t \times 15 \times 100$ mm in dimension, which were sand blasted, ultrasonically cleaned in acetone, and annealed in vacuum at 900 °C for 1 h in order to remove any residual stress caused by the preparation procedures. Other conditions were the same as reported previously.[1]

2.4 Optical Microscopy

Polished cross sections of coated specimens were observed under optical microscope. The Knoop indentation hardness measurement with 100 g load was carried out on the cross sections of the specimens in order to evaluate the degree and depth of work hardening caused by the HVOF particles.

2.5 X-Ray Stress Measurement

X-ray stress measurement was carried out on the surface of the strip-shaped specimens made during the curvature experiments. A Rigaku RINT2000 diffractometer (Tokyo, Japan) was used with a special stress attachment, and a Cr K_α line (30 kV, 200 mA) was employed to measure the (220) peak approximately at $2\theta = 128°$. Ten measurements of 2θ were made at $\Psi = 0, 13, 19, 23, 27, 30, 33, 36, 39, 45°$, and the stress constant -671.6 MPa/° was used. Here, Ψ is the angle between the normal to the coating surface and the normal to the diffracting planes. In order to examine the variation of stress from the coating surface toward inside, the coating was electrochemically etched to remove a layer of about 30 μm thickness and the stress on the new surface was measured after each step of etching.

3. Results and Discussion

3.1 Velocity and Temperature of Sprayed Particles

Figure 2 shows the dependence of both the temperature and the velocity of sprayed particles on the diameter under the operating condition of S2 in the S-series experiment. It needs to be mentioned that the absolute values of the measured temperature are not reliable, as the temperature evaluation depends on the gray body assumption.[8] Since the liquidus temperature of the alloy is around 1700 °C and the observed microstructure indicates that a large portion of sprayed particles before impact were not fully molten, these temperature values must be largely biased to the higher side. However, it is evident that a strong negative correlation exists between the temperature and diameter, whereas the correlation is very weak between the diameter and velocity. Therefore, finer particles are significantly hotter before impact. Such tendency was always evident at the spray distance of 380 mm for other spray conditions in Table 1.

Figure 3 shows the dependence of the average velocity and temperature of particles on the pressure P_c of the combustion chamber. Even though the two plots at $P = 0.69$ MPa are for

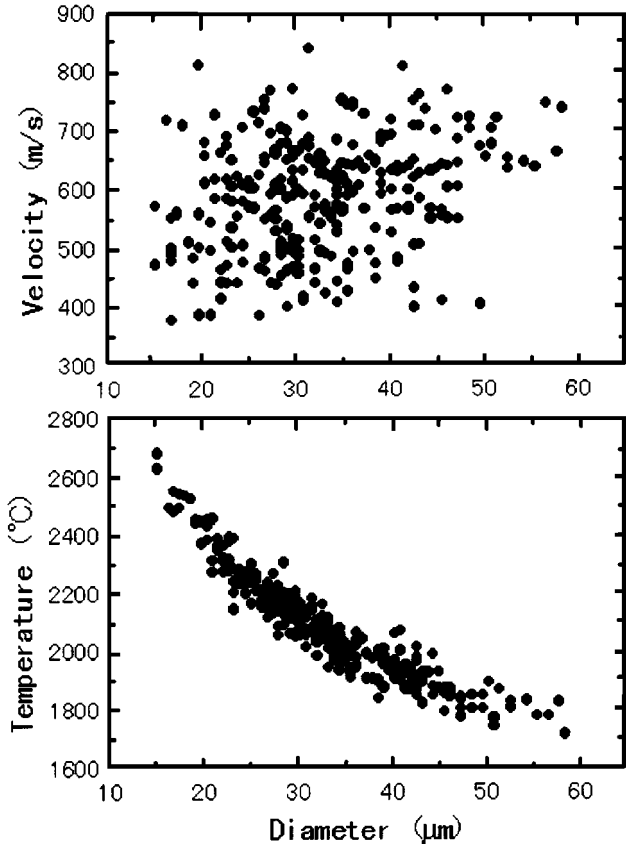

Fig. 2 Correlation of the velocity and temperature of HVOF sprayed particles with diameter under condition S2

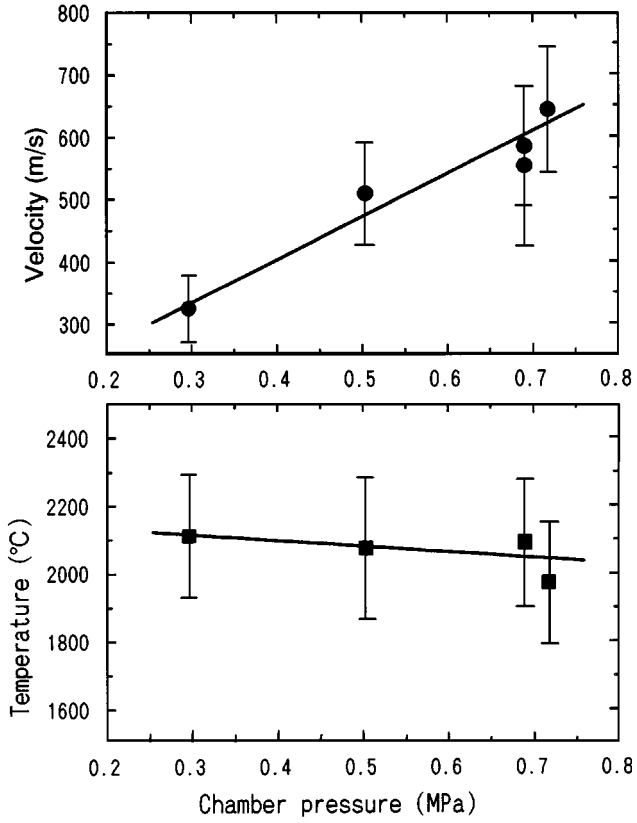

Fig. 3 Dependence of the velocity and temperature of HOVF sprayed particles on the pressure within the combustion chamber

Table 1 List of spray conditions for 316L stainless powders and the thickness of obtained coatings

Condition number	S1	S2	S3	V1	V2	V3
Powder manufacturer	Showa Denko	Showa Denko	Showa Denko	TAFA 1236F	TAFA 1236F	TAFA 1236F
Powder size (μm)	10 to 25	25 to 53	53 to 74	25 to 53	25 to 53	25 to 53
Fuel flow rate (L/min)	0.32	0.32	0.32	0.19	0.30	0.42
Oxygen flow rate (L/min)	853	853	853	351	562	784
Chamber pressure (MPa)	0.69	0.69	0.69	0.30	0.50	0.72
Equivalence fuel/oxygen ratio	0.7	0.7	0.7	1.0	1.0	1.0
Coating thickness (mm)	0.20	0.20	0.09	0.11	0.19	0.19

Barrel length: 102 mm, torch scan velocity: 700 mm/s, torch standoff: 380 mm, powder feed rate: 70 g/min, a powder feed gas: nitrogen

equivalence fuel/oxygen ratio $\Phi = 0.7$ and 1.2 and the other three plots are for $\Phi = 1.0$, it seems that the chamber pressure essentially controls the particle velocity, as reported by Swank *et al.*[7] The average particle velocity markedly increased as the chamber pressure increased, whereas the temperature did not change as much.

3.2 Microstructure and Hardness Distribution

Figure 4 shows the optical micrographs of the polished cross sections of sprayed coatings with different powder sizes, and Fig. 5 shows the effects of chamber pressure on the microstructure. As listed in Table 1, the coating thickness halved for the

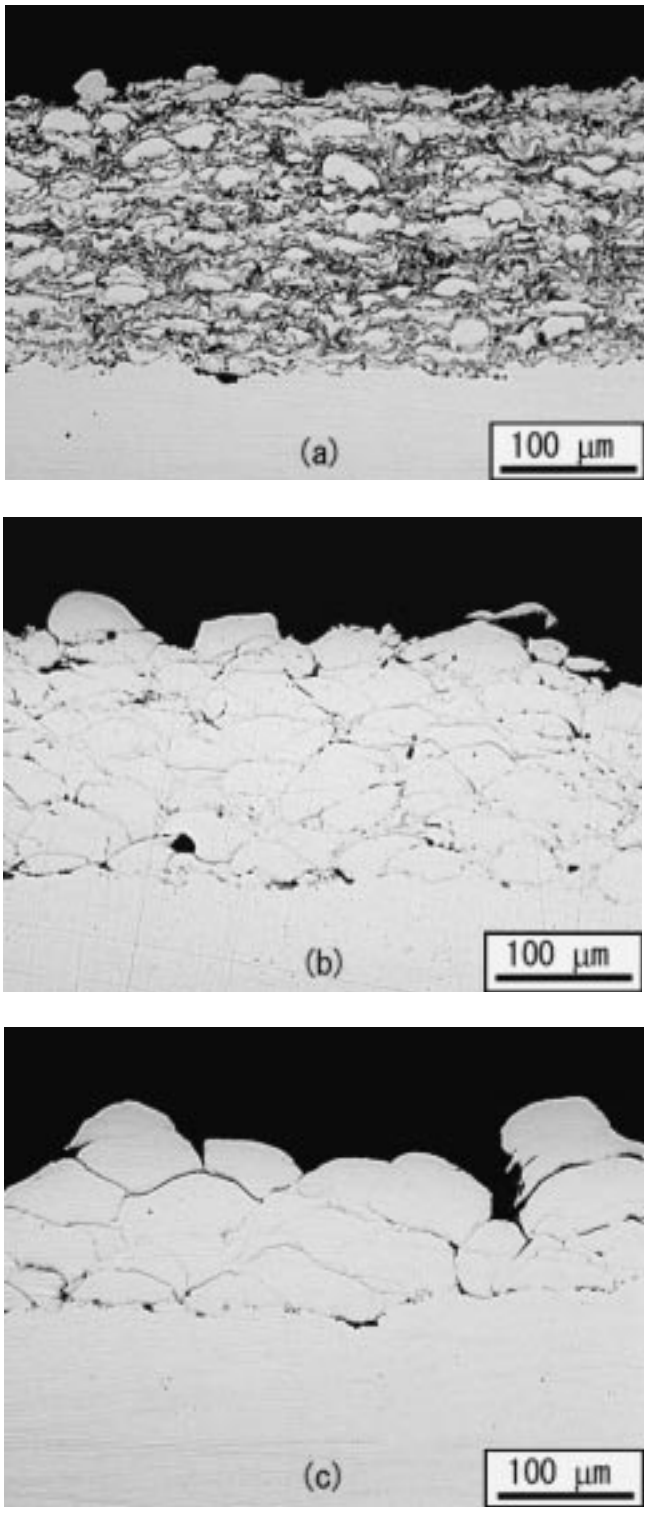

Fig. 4 Polished cross sections of HVOF 316L stainless steel coatings for different powder sizes: (**a**) 10 to 25 μm, (**b**) 25 to 53 μm, and (**c**) 53 to 74 μm

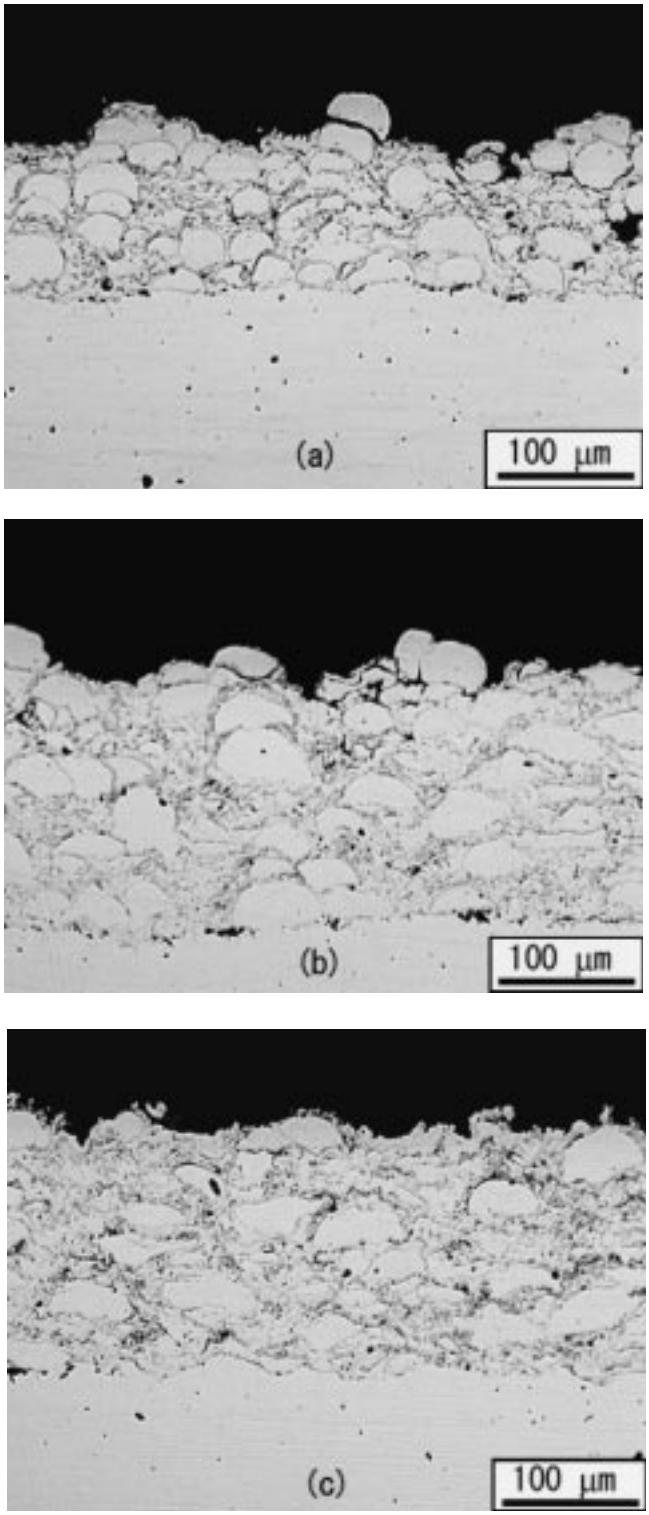

Fig. 5 Polished cross sections of HVOF 316L stainless steel coatings for different chamber pressures: (**a**) 0.3 MPa, (**b**) 0.5 MPa, and (**c**) 0.72 MPa

coarsest powder (S3) and the lowest chamber pressure (V1), whereas it was approximately the same 0.2 mm for the rest. It seems that insufficient heating was the cause of the poor deposition efficiency for the coarsest powder, whereas insufficient velocity was the cause for the lowest P_c. Generally speaking, the coatings consist of two types of microstructures: one has bright, doughy particles, and the other has darker areas with complicated microstructure. The latter is due to the molten phase being

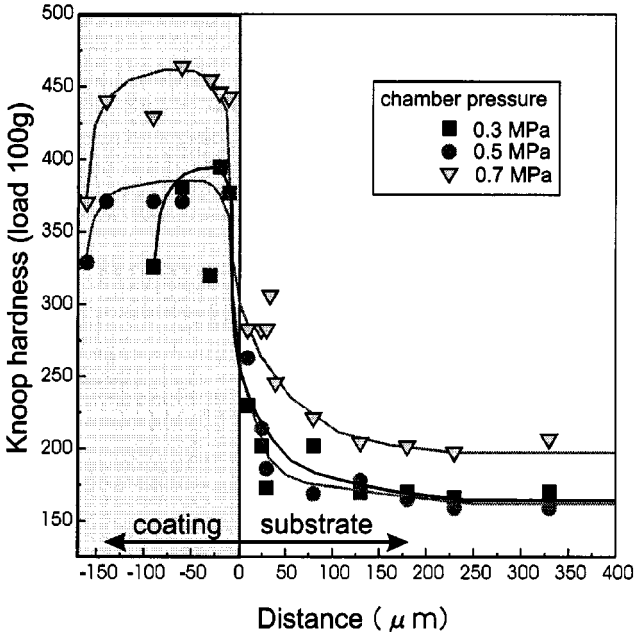

Fig. 6 Distributions of the Knoop hardness across the thickness of HVOF thermal sprayed 316L stainless coatings

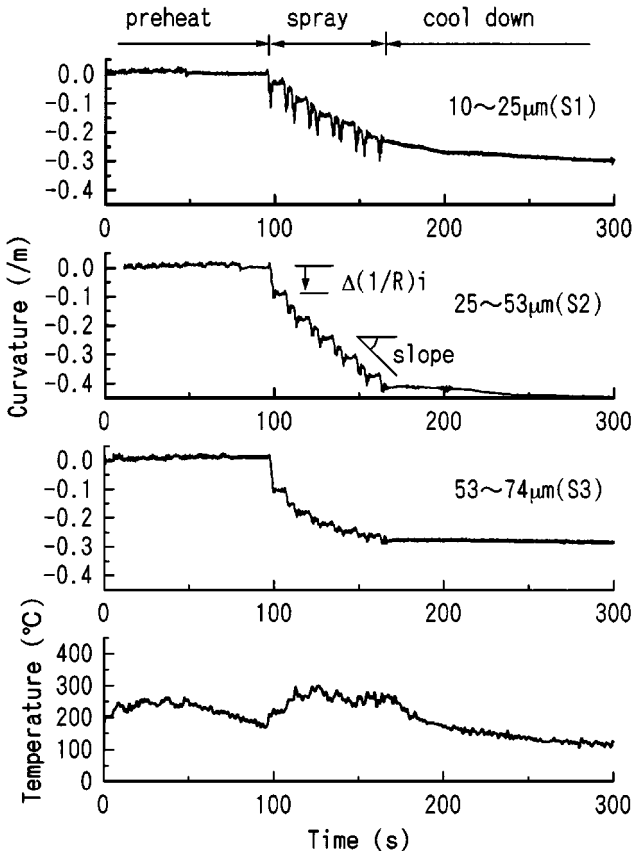

Fig. 7 Curvature and temperature of substrate during HVOF spraying of 316L stainless powder with different powder sizes

disintegrated upon impact, in which the degree of oxidation is high according to Voggenreiter *et al.*[10] In the S series, the coating made of powder below 25 μm has the finest microstructure with well-flattened lamellae and a significant amount of molten phase. With the medium size powder, the amount of molten phase decreased significantly, and it almost completely disappeared with the powder over 53 μm.

In the V series shown in Fig. 5, the degree of flattening of bright unmolten particles increased with P_c. The size of bright particles in V1 was significantly smaller than the other two, even though the same powder was sprayed to prepare these, indicating that the coarser portion of the powder was probably bounced off due to low velocity, which resulted in the low deposition efficiency.

Figure 6 shows the results of the Knoop hardness measurement for the specimens prepared with different chamber pressures (V series). The following characteristics were evident for the hardness distributions of both the V and S specimens, however. The hardness values of the coatings were significantly higher than the substrate, but the surface of the coatings was softer than the inside. Also, there was a layer of increased hardness on the surface layer of substrates below the coatings. This is not due to the sand blasting before spraying because the substrates were annealed before spraying. These observations generally agree with the model shown in Fig. 1(b). This is because the hardness was increased by the work hardening due to the impact of the HVOF particles, and the hardness of the surface of coatings should be lower than the inside because it is not peened by the following particles. The thickness of the hardened layer within substrates gives an approximate value for δ_p, which was more than 50 μm for $P_c = 0.7$ MPa (V3) and decreased with the reduction in P_c.

3.3 Curvature Change and Stress Analysis

Figure 7 and 8 show the measured curvature and temperature changes of substrates during spraying for the S- and V-series conditions, respectively. Even though the temperature change shown in these figures matches the curvature trace just above it, the thermal cycle was approximately the same for the five specimens, except for V3, in which the temperature went up to 350 °C due to the high power of the flame. The curvature changes are characterized by (1) the initial stepwise change at the onset of spraying, (2) the continuous increase during spraying with cyclic oscillations due to the torch motion, and (3) the slight smooth change during cooling after spraying. The negative peaks most evident in S1 during spraying are due to the transient thermal gradient generated by the heat content within the deposited layer. As shown in Fig. 8, the magnitude of the downward peaks decreased with the powder size, which reflects the data in Fig. 3 that the finer particles are hotter before impact.

The slight smooth change in curvature during cooling after spraying implies that the thermal expansivity of the coating is not identical to that of the substrate. The sample bends away from the gun slightly during cooldown, though the degree of such action depends on the spray condition. This implies a smaller expansivity of the deposit than the substrate. A higher oxide content in the coating might be expected to reduce the coefficient of thermal expansion of the coating. In the S series, the

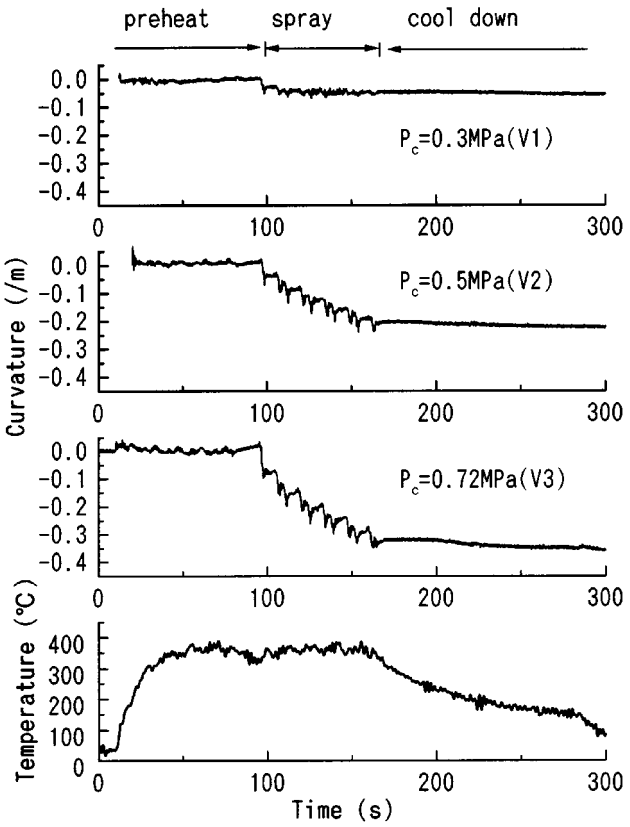

Fig. 8 Curvature and temperature of substrate during HVOF spraying of 316L stainless powder with different chamber pressures

cooldown deflection is greatest where the powder size is smallest. In the V series, it is greatest where the particle velocity is highest. These are the coatings with the largest amount of molten material, and thus oxide, in each series.

Another important characteristic in the curvature traces is that, in some cases, the rate of curvature change decreased significantly as the coating thickness increased. Such tendency is evident in S1, S3, and V1. As the coating thickness increases, the flexural stiffness of the substrate-coating couple increases. If an addition of a new layer of sprayed deposit brings in the same level of stress on the top layer throughout the spraying period, this should result in the gradual decrease in the slope of curvature change. The maximum coating thickness in these experiments was 200 μm and the substrate thickness was 2 mm. Assuming the elasticity of the coating to be equal to the substrate, approximately 20% increase in the flexural stiffness is expected. Therefore, the difference in the slope between the beginning and the end of the spraying period due to the thickness effect is estimated as 20% at maximum. The observed changes in the slope for these three cases are much more than 20% and some other reasons must be sought.

At the beginning of spraying, the target is a bare substrate of annealed 316L steel, upon which the introduction of compressive stress is most effective. As the coating with greater hardness is built upon, however, the efficiency of stress generation should gradually decrease, which is probably what is happening in S1 and V1. In the case of S3, it seems that the saturation in the stress

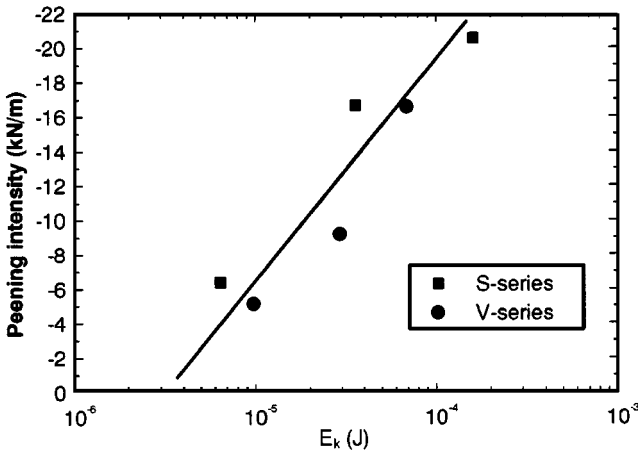

Fig. 9 Correlation between the peening intensity I_p and the average kinetic energy E_k of HVOF thermal sprayed particles upon impact. The S series has different powder sizes and the V series is for different chamber pressures

generation was taking place because of the slow rate of coating thickness increase coupled with the high impact energy due to large particles. When the coating growth rate and the stress generation were balanced from the beginning, curvature increased linearly with time.

For more quantitative analysis, the initial change in curvature at the onset of spraying $\Delta(1/R)_i$, as shown in Fig. 7 (S2), was taken, first, as a measure of the peening intensity of the HVOF particles. The peening intensity I_p (N/m) is defined and evaluated as

$$I_p = \int_\tau^0 \sigma dz \cong \frac{1}{6}\frac{E_S(T_S)h_S^2}{(1-\nu)}\Delta\left(\frac{1}{R}\right)_i \quad \text{(Eq 1)}$$

Here, the stress σ in Fig. 1(b) is integrated over the distance from the surface of splats and is evaluated by Stoney's formula assuming that the depth of stress distribution is sufficiently small as compared to the substrate thickness. $E_s(T_s)$ is the Young's modulus at the substrate temperature T_s, h_s is the thickness, and ν is the Poisson's ratio of the substrate. Thus, evaluated values of I_p were correlated with the average kinetic energy i of HVOF sprayed particles. The value of E_k was calculated by the following formula using the data collected by DPV2000, where N is the number of particles, m is the mass of each particle calculated by the density of the powder material and the diameter, and v is the velocity.

$$E_k = \frac{1}{N}\sum_{n=1}^{N}\frac{1}{2}mv^2 \quad \text{(Eq 2)}$$

As might be expected, almost linear dependence of I_p on log (E_k) was found, as shown in Fig. 9.

Second, the steady-state deposition stress σ_{ss} is evaluated from the slope of the curvature change at the end of the spraying period, as shown in Fig. 7 (S2) by the following equation:

$$\sigma_{ss} = \frac{1}{6}\frac{E_s(T_s)(h_s+h_c)^2}{(1-\nu)}\frac{\partial}{\partial h_c}\left(\frac{1}{R}\right) \quad \text{(Eq 3)}$$

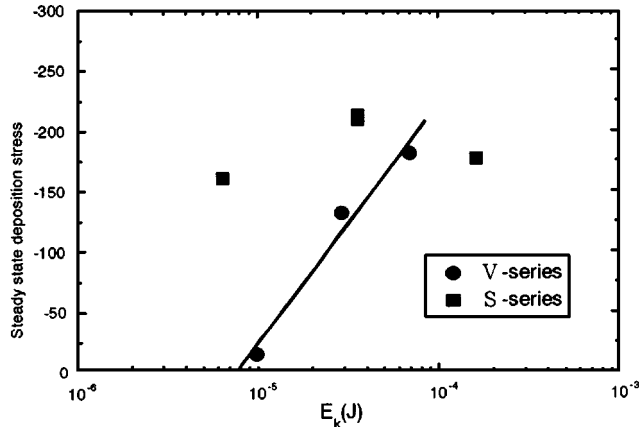

Fig. 10 Dependence of the steady-state deposition stress σ_{ss} on the average kinetic energy E_k of HVOF thermal sprayed particles upon impact. The S series has different powder sizes and the V series is for different chamber pressures

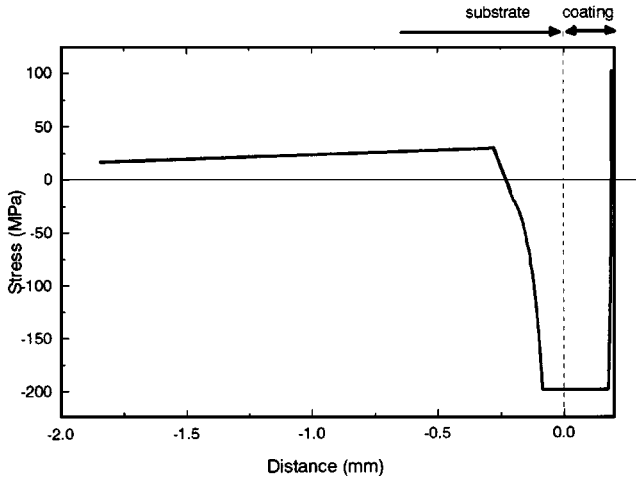

Fig. 11 An example of expected stress distribution in 316L stainless steel coatings HVOF sprayed on a 316L steel substrat

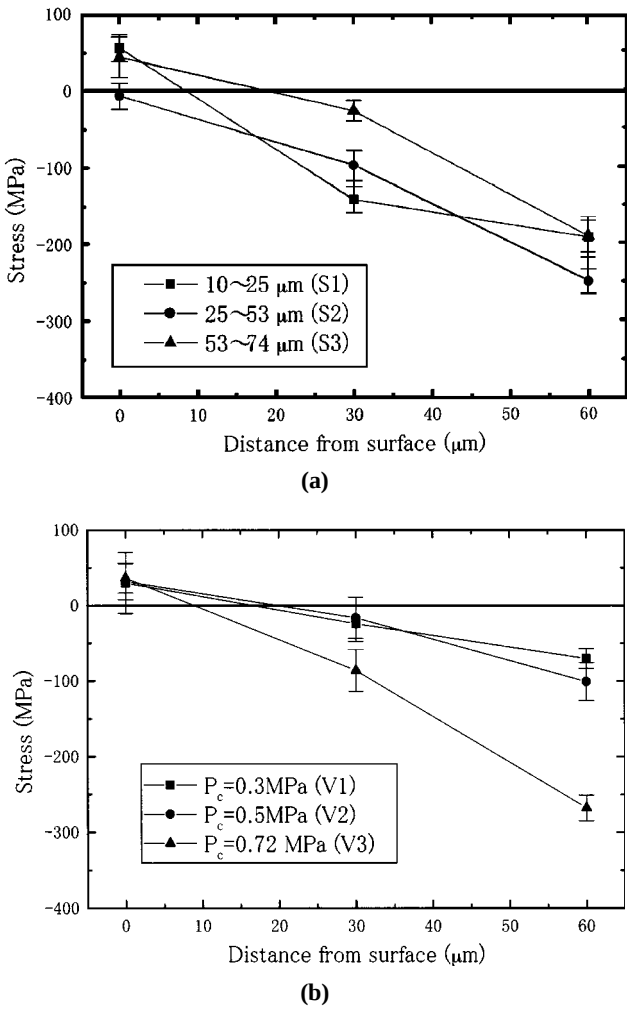

Fig. 12 Stress distributions from the coating surface obtained by the x-ray stress measurement: (**a**) S series with different powder sizes and (**b**) V series for different chamber

where σ_{ss} is the average value of the stress induced by depositing a new layer on top of the already deposited coating, and in the steady state, the coating is so thick that the substrate is not affected any more. Therefore, σ_{ss} is a function of both the state of the impinging particles and the coating, but is independent of the substrate material, just like the quenching stress for molten particles. The significant difference, however, is that the transition to the steady state may require the coating to be thicker than 50 μm due to the high penetrating power of the HVOF sprayed particles, as shown by the hardness measurement in Fig. 6. As shown in Fig. 10, there is not a clear correlation between σ_{ss} and E_k as a whole, but for the V series, where the coatings were made of the same powder, there seems to be a good correlation, as depicted by a straight line in the figure.

Finally, stress distribution through thickness needs to be discussed. An example of expected stress distribution within a coating is calculated and shown in Fig. 11. The calculation was done for $\sigma_q = 100$ MPa, $\sigma_p = -200$ MPa, $\delta_p = 50$ μm, and the yield stress of 316L steel $\sigma_y = 200$ MPa, assuming a complete elastic-plastic behavior and the substrate to be much thicker than the 200 μm thick coating. Such prediction, however, needs to be tested by other methods such as the x-ray and layer removal techniques. Results of x-ray stress measurement are shown in Fig. 12(a) and (b) for the S series and V series, respectively. Both data show that the surface of the coating is in most cases stressed in a weak tension, but the stress within the coating deeper than 50 μm is in significant compression. Because the penetration depth of the x-ray is approximately 25 μm and is comparable with the surface roughness of the coating, the stress values measured on the coating surface must reflect significantly relaxed values due to the free surfaces inclined to the coating plane.[4] Nevertheless, the reversal of the sign of stress from the top layer to the inside coincides with the prediction given in Fig. 11. Similar tensile stresses on the surface of HVOF sprayed MCrAlY alloys were measured by the x-ray method.[11] Figure 12(b) shows that higher combustion pressure generated higher compressive stresses within the coatings, whereas correlation is not so obvious between the stress level and the powder size, as shown in Fig. 12 (a).

4. Conclusions

The process of stress generation in HVOF sprayed coatings is more complicated as compared to conventional thermal spray processes because of the peening action of the high-velocity particles, which introduces significant compressive stress within and beneath the deposited layer. For the process studied, the depth of the peening effect could be as deep as 50 μm. By using the *in-situ* curvature measurements and the particles diagnostics, the intensity of peening action was directly correlated with the kinetic energy of the sprayed particles. At the onset of spraying, when the substrate is peened, the peening intensity was found to increase with the kinetic energy of sprayed particles. The peening stress in the steady state depended on the properties of both the coating and the sprayed particles, and the stress value ranged from 200 MPa to an almost negligible level. These results indicate that a broad window for stress control is available through the control of spray parameters with the HVOF processes.

Acknowledgment

Mr. M. Sasaki, Plasma Giken Co., is gratefully acknowledged for his technical assistance during the HVOF experiments.

References

1. S. Kuroda, Y. Tashiro, H. Yumoto, S. Taira, and H. Fukanuma: in *Thermal Spray: United Forum Scientific Technological Advances*, C.C. Berndt, ed., ASM International, Materials Park, OH, 1997, pp. 805-11.
2. Y. Itoh, M. Saitoh, and M. Tamura: *Trans. Jpn. Soc. Mech. Eng. (A)*, 1997, vol. 63, pp. 1979-85 (in Japanese).
3. S. Kuroda and T.W. Clyne: *Thin Solid Films*, 1991, vol. 200, pp. 49–66.
4. S. Kuroda, T. Fukushima, and S. Kitahara: *J. Thermal Spray Technol.*, 1992, vol. 1, pp. 325-32.
5. T.W. Clyne and S.C. Gill: *J. Thermal Spray Technol., Residual Stresses Thermal Spray Coatings*, 1996, vol. 5, pp. 401-18.
6. Y.C.Tsui and T.W. Clyne: in *Thermal Spray: A United Forum Scientific Technological Advances*, C.C. Berndt, ed., ASM International, Materials Park, OH, 1997, pp. 813-22.
7. W.D. Swank, J.R. Fincke, D.C. Haggard, G. Irons, and R. Bullock: in *Thermal Spray Industrial Applications*, C. C. Berndt and S. Sampath, eds., ASM International, Materials Park, OH, 1994, pp. 319-24.
8. C.P. Moreau, P. Gougeon, and M. Lamontagne: in *Thermal Spraying—Current Status and Future Trends*, A. Ohmori, ed., High Temperature Society of Japan, Osaka, Japan, 1995, pp. 347-51.
9. S. Kuroda, T. Fukushima, and S. Kitahara: *Thin Solid Films*, 1988, vol. 164, pp. 157-63.
10. H. Voggenreiter, H. Huber, S. Beyer, and H.J. Spies: in *Advances in Thermal Spray Science and Technology*, C.C. Berndt and S. Sampath, eds., ASM International, Materials Park, OH, 1995, pp. 303-08.
11. Y. Itoh, M. Saitoh, and M. Tamura: *J. Soc. Mater. Sci., Jpn.*, 1997, vol. 46, pp. 1057-63 (in Japanese).